Weighted stacking of 3-D converted-wave data for birefringent media

Richard A. Bale

ABSTRACT

This paper describes a proposed method for weighted stacking of 3-D converted-wave data to give geometry-independent estimates of the S1 and S2 wavefields in the presence of shear-wave splitting. The method can also account for offset dependent amplitudes, which generally cannot be neglected for converted-wave data. The stacking procedure uses an estimate of the principal axis direction, but does not require information on the propagation differences between S1 and S2 modes. The stack normalization scalars are dependent on both acquisition geometry and principal axis direction. These are computed for a simple cross-spread example, to derive S1 and S2 "effective fold" maps. The maps show features that are related to the interplay between geometry and principal axis direction.

INTRODUCTION

One of the promises of multicomponent seismic is the ability to characterize fractured reservoirs, using the sensitivity of shear-waves to azimuthal anisotropy – in particular the phenomenon of shear-wave "splitting" or birefringence. Birefringence can arise due to the presence of vertically aligned cracks in the medium or possibly due to the presence of preferential stress directions. Whilst azimuthal anisotropy has an impact on compressional waves both in terms of moveout and AVO variation with azimuth, it may be more readily detected from shear-wave data. In shear-wave birefringence the shear-waves propagate through the anisotropic medium with two distinct polarizations with different velocities, leading to the designation of a "fast" (S1) wave and a "slow" (S2) wave. The identification of these two polarizations and velocities has been the subject of much recent work (e.g. Garotta, 1989; Gaiser, 2000). These and other workers have shown that 3-D converted-wave data may be used instead of the traditional 2-D approach requiring two orthogonally polarized shear-wave sources (Alford, 1986; Thomsen, 1988).

Beyond estimation of polarizations, lies the goal of imaging of S1 and S2 modes. In order properly to image converted-wave data in the presence of shear-wave splitting, it is important to consider the kinematic and dynamic variations with polarization. Failure to do so can result in poor resolution and incorrect amplitudes (Probert and Wells, 2000). Simple imaging of the 3-D radial component, valid for azimuthal isotropy, fails to the degree anisotropy is present. Shear-wave splitting combined with spatial variations in the azimuth distribution result in an exacerbation of the usual acquisition footprint problems encountered with 3-D surveys. One approach is to remove the kinematic and dynamic effect of the anisotropy by "layer stripping" and recombine the modes to form an "isotropic" radial component image. However, the P-S1 and P-S2 amplitudes are potentially different and independently of interest. The goal of this paper is to formulate a practicable theoretical basis for determining separate P-S1 and P-S2 images from the 3-D data.

THEORY

Figure 1 depicts a layered medium containing a single anisotropic layer, resulting from vertically aligned cracks or stress field. The converted-waves can interact in three possible ways with the anisotropic layer. In case A, the wave is converted from the top of the anisotropic layer. This results in a transverse (out of plane) amplitude response, but not in any splitting, since there is no propagation through the layer itself. The effect is fairly benign, in the sense that there is no kinematic variation with azimuth, which would tend to degrade the imaging. In case B the wave is converted by a reflector below the anisotropic layer, giving rise to an initially radial shear-wave, which then becomes split upon transmission through the anisotropic layer. In this case, the associated travel-time delay differences can degrade the image if unaccounted for. Finally, in case C we get a mixture of these two effects, with both reflection and propagation being influenced by the anisotropy layer. In this paper I am considering case B.

Figure 2 shows the relationship between the source-receiver geometry, the principal axes (i.e. S1 and S2 directions) of the medium, and the *X*-*Y* coordinate frame. Here it is assumed that the in-line and cross-line geophone have been aligned along the *X* and *Y* axes respectively.

The splitting behaviour of the converted-wave B shown in Figure 1 can be formulated in the frequency domain as follows (after Li, 1998):

$$\begin{pmatrix} X(\omega) \\ Y(\omega) \end{pmatrix} = \mathbf{R}(\phi) \begin{pmatrix} f_1(\omega) e^{-i\omega\tau_1} & 0 \\ 0 & f_2(\omega) e^{-i\omega\tau_2} \end{pmatrix} \mathbf{R}(\theta - \phi) \begin{pmatrix} U_{PS}(\omega) \\ 0 \end{pmatrix} \qquad (1)$$

where *X* and *Y* are the recorded wavefields for in-line and cross-line component geophones respectively, θ is the azimuth between the source-receiver azimuth and the *X*-axis, and ϕ is the azimuth between the fast shear-wave (S1) direction and the *X*-axis. **R** is a rotation matrix given by:

$$\mathbf{R}(\theta) = \begin{pmatrix} \cos\theta & -\sin\theta \\ \sin\theta & \cos\theta \end{pmatrix} \text{ with inverse } \mathbf{R}^T(\theta) = \mathbf{R}^{-1}(\theta) = \begin{pmatrix} \cos\theta & \sin\theta \\ -\sin\theta & \cos\theta \end{pmatrix}$$

$U_{PS}(\omega)$ needs a bit of explanation. Here it is taken to be the wavefield immediately after mode conversion at point CP (Figure 1). It includes the P-wave propagation effects, the AVO response of the reflection (the reason for including this will become apparent), but *not* any shear-wave propagation effects. The terms $f_1(\omega)$ and $f_2(\omega)$ describe propagation along the S1 and S2 directions respectively, including any pure SV leg prior to splitting. Moving from right to left, equation (1) shows a converted-wave, initially polarized in the radial direction, being decomposed into orthogonal shear-wave modes polarized in the S1 and S2 directions, each mode propagating with different time delays and different transmission responses through the anisotropic layer, then being recorded by horizontal components in the *X* and *Y* directions. I note in passing that if $f_1 = f_2$ and $\tau_1 = \tau_2$, corresponding to the isotropic case, then the diagonal matrix in equation (1) is a scaled identity matrix. In this case

the rotation matrices can be multiplied directly to obtain a simple rotation, $\mathbf{R}(\theta)$, which corresponds to mapping from source-receiver to acquisition coordinates, and can be simply inverted by the usual radial rotation $\mathbf{R}^T(\theta)$.

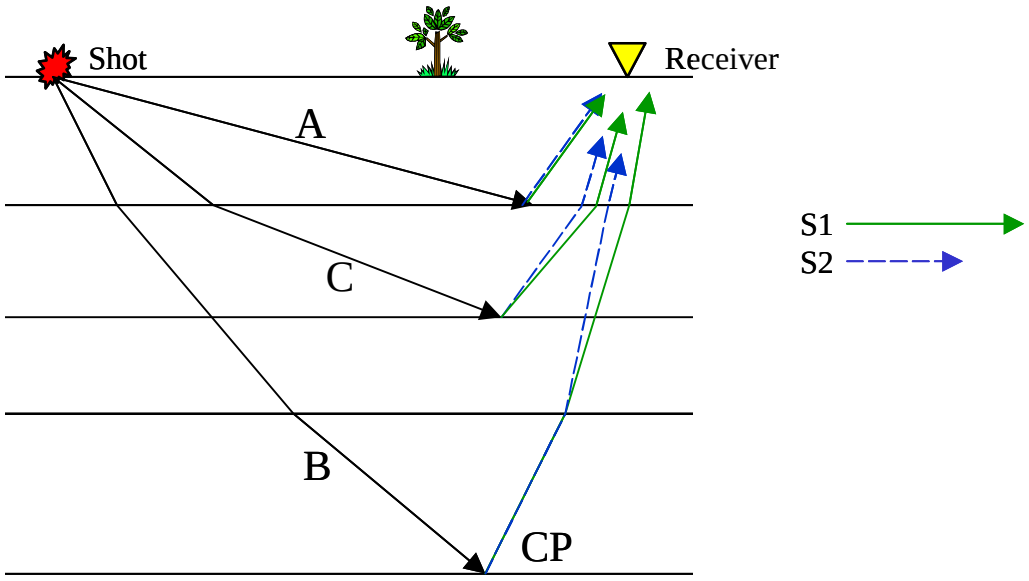

FIG. 1. Recording of birefringent shear-waves from converted-wave acquisition. Shaded area depicts an azimuthally anisotropic layer. Event A, from top of the anisotropic layer, has an azimuthal reflection response effect. Event B, reflected from below the anisotropic layer, has both azimuthal traveltime and transmission response effects. Event C has reflection response, transmission response and traveltime effects.

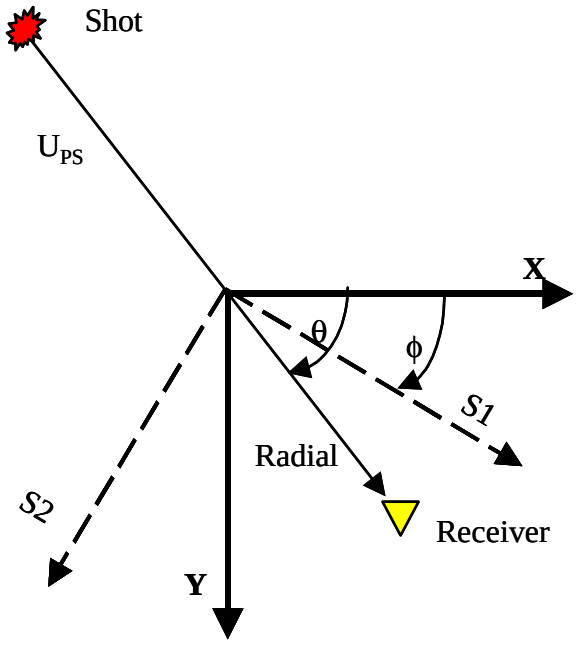

FIG. 2. Schematic diagram of surface geometry, showing azimuths of radial (shot-receiver) direction and principal axes (S1 and S2) relative to XY receiver coordinate system.

Li (1998) considered the 3-D behaviour of equation (1), and showed that the transverse component undergoes polarity reversal when θ crosses the S1 and S2 azimuths, ϕ and $\phi + 90^\circ$. This property may be used (Bale et al., 2000) as a "detector" of the S1 azimuth.

Equation (1) may also be written in the following form:

$$\begin{pmatrix} X(\omega) \\ Y(\omega) \end{pmatrix} = \mathbf{R}(\phi) \begin{pmatrix} \cos(\theta-\phi) U_{PS1}(\omega) \\ \sin(\theta-\phi) U_{PS2}(\omega) \end{pmatrix}$$
$$\begin{pmatrix} U_{PS1}(\omega) \\ U_{PS2}(\omega) \end{pmatrix} = \begin{pmatrix} f_1(\omega) e^{-i\omega\tau_1} U_{PS}(\omega) \\ f_2(\omega) e^{-i\omega\tau_2} U_{PS}(\omega) \end{pmatrix} \qquad (2)$$

When deciding on the inverse problem, it is important to decide what we wish to recover from equation (2). Obviously one possible answer is $U_{PS}(\omega)$, the wavefield at the reflector after removing the propagation effects of the birefringence. This is the approach taken by Gaiser (2000) and others, whereby the difference between S1 and S2 modes is removed in order to recombine them into a single "radial" response. In some cases, however, we may wish to retain independent results from the split shear-waves, particularly, perhaps, where there may be some difficulty removing the effects of the S1 and S2 responses, or where we want to look at S1 and S2 reflectivity. In this case, it is desirable to recover $U_{PS1}(\omega)$ and $U_{PS2}(\omega)$, which describe the earth's response to P-waves generated in the fast and slow directions respectively. It is important to note that these *exclude* the rotation terms, which are acquisition dependent, resulting from the choice of source and receiver positions. It is also important to note that we do *not* recover $U_{PS1}(\omega)$ and $U_{PS2}(\omega)$ by simply rotating to the principal (S1 and S2) axes, using $\mathbf{R}^T(\phi)$.

For a single trace, the inverse equation is quite straightforward:

$$\begin{pmatrix} U_{PS1}(\omega) \\ U_{PS2}(\omega) \end{pmatrix} = \begin{pmatrix} 1/\cos(\theta-\phi) & 0 \\ 0 & 1/\sin(\theta-\phi) \end{pmatrix} \mathbf{R}^T(\phi) \begin{pmatrix} X(\omega) \\ Y(\omega) \end{pmatrix} \qquad (3)$$

However, this will generally not be the optimal approach for multifold data, as it will tend to amplify noise along the principal directions, where $\theta = \phi$.

Stacking

In a 3-D multicomponent survey, the converted-wave (usually horizontal component) data are stacked together based upon their common conversion point (CCP) location (Tessmer and Behle, 1988; Thomsen, 1999). I assume here that the same conversion-point binning is valid for both S1 and S2 modes, though note that in general it may not be, if the difference in velocities is significant. Consider an arbitrary bin

containing both *X*-component and *Y*-component traces $i=1,\ldots,N$, each with different shot and receiver coordinates, which are to be stacked (as illustrated in Figure 3). Which parts of equation (1) are expected to be a function of the shot and receiver locations? If it is assumed that $U_{PS1}(\omega)$ and $U_{PS2}(\omega)$ are offset-independent (a dubious assumption which is revisited in the next section), then the only dependence on geometry is through θ.

We thus have:

$$\begin{pmatrix}\cos(\theta_i-\phi)U_{PS1}(\omega)\\ \sin(\theta_i-\phi)U_{PS2}(\omega)\end{pmatrix}=\mathbf{R}^T(\phi)\begin{pmatrix}X_i(\omega)\\ Y_i(\omega)\end{pmatrix}=\begin{pmatrix}A_{S1,i}(\omega)\\ A_{S2,i}(\omega)\end{pmatrix}$$

$$A_{S1,i}(\omega)=\cos(\phi)X_i(\omega)+\sin(\phi)Y_i(\omega)$$
$$A_{S2,i}(\omega)=-\sin(\phi)X_i(\omega)+\cos(\phi)Y_i(\omega) \qquad (4)$$

These are actually two decoupled sets of *N* equations each for the two unknowns $U_{PS1}(\omega)$ and $U_{PS2}(\omega)$, which can be written as two least squares problems:

$$\mathbf{L}_1^T\mathbf{A}_{S1}(\omega)=(\mathbf{L}_1^T\mathbf{L}_1)U_{PS1}(\omega)$$
$$\mathbf{L}_2^T\mathbf{A}_{S2}(\omega)=(\mathbf{L}_2^T\mathbf{L}_2)U_{PS2}(\omega) \qquad (5)$$

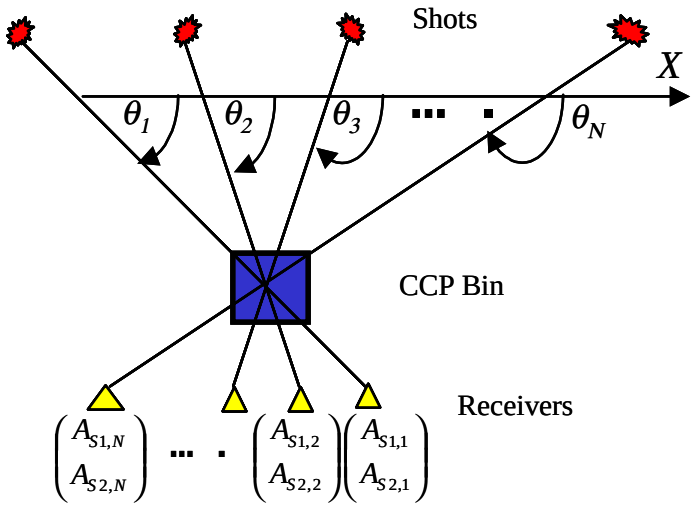

FIG. 3. CCP binning geometry. $A_{S1,i}$ and $A_{S2,i}$ are amplitudes of S1 and S2 for θ_i. Azimuth variation of traces contributing to the CCP stack leads to geometry dependent amplitude effects.

$$\text{where } \mathbf{L}_1 = \begin{pmatrix} \cos(\theta_1 - \phi) \\ \cos(\theta_2 - \phi) \\ \cos(\theta_3 - \phi) \\ \vdots \\ \cos(\theta_N - \phi) \end{pmatrix}, \mathbf{L}_2 = \begin{pmatrix} \sin(\theta_1 - \phi) \\ \sin(\theta_2 - \phi) \\ \sin(\theta_3 - \phi) \\ \vdots \\ \sin(\theta_N - \phi) \end{pmatrix}, \mathbf{A}_{S1} = \begin{pmatrix} A_{S1,1} \\ A_{S1,2} \\ A_{S1,3} \\ \vdots \\ A_{S1,N} \end{pmatrix} \text{and } \mathbf{A}_{S2} = \begin{pmatrix} A_{S2,1} \\ A_{S2,2} \\ A_{S2,3} \\ \vdots \\ A_{S2,N} \end{pmatrix}$$

These are trivially inverted to yield the required P-S1 and P-S2 wavefields, as weighted stacks:

$$U_{PS,1}(\omega) = \frac{\sum_{i=1}^{N} \cos(\theta_i - \phi) A_{S1,i}(\omega)}{\sum_{i=1}^{N} \cos^2(\theta_i - \phi)} \text{ and } U_{PS,2}(\omega) = \frac{\sum_{i=1}^{N} \sin(\theta_i - \phi) A_{S2,i}(\omega)}{\sum_{i=1}^{N} \sin^2(\theta_i - \phi)}. \quad (6)$$

The weighting coefficients are interesting in themselves, as they contain important information about the geometry of the survey relative to the principal axes. For example, the sums in the denominators may be interpreted as a kind of "effective fold" for S1 and S2, as shown below in the "Example" section.

Equation (6) was derived and applied to a synthetic dataset by Bale et al. (2000).

Offset dependence

Converted-waves are subject to a strong AVO effect, which is approximately sinusoidal at small incidence angles. Unless the offsets being stacked are very similar, (e.g. if stacking is being performed in offsets bands) the assumption of offset dependence made above is unjustified.

The relationship between P-S reflectivity and S-S reflectivity for small angles ($< 20^\circ$) is given by (Stewart et al., 1995):

$$R^{PS} = 4 p V_S R^{SS} \quad (7)$$

where $p = dt/dx$ is the ray parameter, and V_S is the interval shear velocity averaged across the reflector.

To incorporate the angle dependence into the birefringent stacking correction, we make the following substitution:

$$U_{PS}(\omega, p) = 4 p V_S U_{SS}(\omega, 0). \quad (8)$$

The assumption here is that U_{SS} may be treated as an offset- (and azimuth-) independent response (though it is not strictly speaking a shear-wave earth response, since the downward propagation is a P-wave). Updating equation (4) and labeling the ray-parameters for different traces p_i, (i=1,…,N) we obtain:

$$4V_S\begin{pmatrix}\cos(\theta_i-\phi)p_iU_{SS1}(\omega)\\ \sin(\theta_i-\phi)p_iU_{SS2}(\omega)\end{pmatrix}=\mathbf{R}^T(\phi)\begin{pmatrix}X_i(\omega)\\ Y_i(\omega)\end{pmatrix}=\begin{pmatrix}A_{S1,i}(\omega)\\ A_{S2,i}(\omega)\end{pmatrix} \tag{9}$$

where the natural definitions of the (geometry-independent) fast and slow shear-wave wavefields $U_{SS1,2}$ are:

$$\begin{pmatrix}U_{SS1}(\omega)\\ U_{SS2}(\omega)\end{pmatrix}=\begin{pmatrix}f_1(\omega)e^{-i\omega\tau_1}U_{SS}(\omega,0)\\ f_2(\omega)e^{-i\omega\tau_2}U_{SS}(\omega,0)\end{pmatrix}$$

Setting up the least squares equation for $U_{SS1,2}$, we obtain:

$$\begin{aligned}\frac{1}{4V_S}\mathbf{M}_1^T\mathbf{A}_{S1}(\omega)&=(\mathbf{M}_1^T\mathbf{M}_1)U_{SS1}(\omega)\\ \frac{1}{4V_S}\mathbf{M}_2^T\mathbf{A}_{S2}(\omega)&=(\mathbf{M}_2^T\mathbf{M}_2)U_{SS2}(\omega)\end{aligned} \tag{10}$$

where $\mathbf{M}_1=\begin{pmatrix}p_1\cos(\theta_1-\phi)\\ p_2\cos(\theta_2-\phi)\\ p_3\cos(\theta_3-\phi)\\ \vdots\\ p_N\cos(\theta_N-\phi)\end{pmatrix}=\mathbf{DL}_1$ and $\mathbf{M}_2=\begin{pmatrix}p_1\sin(\theta_1-\phi)\\ p_2\sin(\theta_2-\phi)\\ p_3\sin(\theta_3-\phi)\\ \vdots\\ p_N\sin(\theta_N-\phi)\end{pmatrix}=\mathbf{DL}_2$

for $\mathbf{D}=diag(p_1,p_2,p_3,...,p_N)$

The solution to equation (10) is given by:

$$U_{SS1}(\omega)=\frac{1}{4V_S}\frac{\sum_{i=1}^{N}p_i\cos(\theta_i-\phi)A_{S1,i}(\omega)}{\sum_{i=1}^{N}p_i^2\cos^2(\theta_i-\phi)}$$

and

$$U_{SS2}(\omega)=\frac{1}{4V_S}\frac{\sum_{i=1}^{N}p_i\sin(\theta_i-\phi)A_{S2,i}(\omega)}{\sum_{i=1}^{N}p_i^2\sin^2(\theta_i-\phi)} \tag{11}$$

Equation (11) suggests a solution in the frequency/ray-parameter domain. Indeed this may be possible. However, in general the sampling along any specified azimuth is insufficient from typical 3-D geometries to generate the required radon transform. An alternative is to recast equation (11) in the space-time domain.

The ray parameter may be computed from a suitable moveout equation, under an assumption of layered media. For example we could use the standard NMO equation, $t^2 = t_0^2 + r^2/V_{PS2}^2$, with zero-offset time t_0, finite-offset time t, source-to-receiver offset r, and converted-wave stacking velocity V_{PS2} (following Walden, 1991), to give:

$$p = \frac{r}{t(r)V_{PS2}^2} = \frac{r}{V_{PS2}^2\sqrt{t_0^2 + r^2/V_{PS2}^2}} \tag{12}$$

Higher order approximations are also possible (Bale et al., 2001; Nieto and Stewart, 2001), but for consistency would require parameterization of AVO with a two-term equation instead of (7). For this analysis, I consider only small angle approximations implied by (7) and (12).

Applying an inverse Fourier transform to equation (11), and substituting equation (12) into it, we get:

$$U_{SS1}(t_0) = \frac{V_{PS2}^2}{4V_S}\frac{\sum_{i=1}^{N}\left(\frac{r_i}{t(r_i)}\right)\cos(\theta_i - \phi)A_{S1,i}(r_i, t_0)}{\sum_{i=1}^{N}\left(\frac{r_i}{t(r_i)}\right)^2\cos^2(\theta_i - \phi)}$$

and

$$U_{SS2}(t_0) = \frac{V_{PS2}^2}{4V_S}\frac{\sum_{i=1}^{N}\left(\frac{r_i}{t(r_i)}\right)\sin(\theta_i - \phi)A_{S2,i}(r_i, t_0)}{\sum_{i=1}^{N}\left(\frac{r_i}{t(r_i)}\right)^2\sin^2(\theta_i - \phi)} \tag{13}$$

Algorithm

The algorithm implied by equation (13) consists of the following steps:

1. Apply NMO with velocity V_{PS2}.
2. Rotate X and Y component data to principal axes, using $\mathbf{R}^T(\phi)$.
3. Apply weighted stacks based upon $r/t = r/\sqrt{t_0^2 + r^2/V_{PS2}^2}$ multiplied by the cosine (S1) or sine (S2) of the radial azimuth relative to the S1 direction.
4. Normalize by sum of squared weights.
5. Poststack multiply amplitudes by $V_{PS2}^2/4V_S$.

These are all fairly straightforward modifications of standard processing steps applied to 3-D converted-wave data. The only additional burden is keeping track of the weighting functions in order to apply poststack normalization.

Special case: 2-D geometry

In the 2-D case, $\theta = 0$, and we have a rotation which is constant for each trace (Fang and Brown, 1996; Fang, 1998). This situation is more difficult from the point of view of estimation, as the variation with azimuth is unavailable, but simplifies the stacking problem, as the X and Y components may be independently stacked, since the same rotation will be applied to all traces. This can be seen by substituting $\theta = 0$ in equation (13), to give:

$$U_{SS1} = \frac{V_{PS2}^2}{4V_S \cos(\phi)} \frac{\sum_{i=1}^{N} \left(\frac{r_i}{t(r_i)} \right) A_{S1,i}}{\sum_{i=1}^{N} \left(\frac{r_i}{t(r_i)} \right)^2}$$

and

$$U_{SS2} = \frac{-tV_{PS2}^2}{4V_S \sin(\phi)} \frac{\sum_{i=1}^{N} \left(\frac{r_i}{t(r_i)} \right) A_{S2,i}}{\sum_{i=1}^{N} \left(\frac{r_i}{t(r_i)} \right)^2}. \qquad (14)$$

Thus for 2-D data, we have an AVO type weighted stack, divided by a constant cosine or sine of the S1 azimuth relative to the in-line direction. This is just an overall scaling factor, which could be neglected unless comparing the S1 and S2 amplitudes with each other.

EXAMPLE: S1-S2 FOLD ANALYSIS

For isotropic processing, the converted-wave stack is normalized by the CCP fold, which is a simple count of the traces falling into the bin before stack. It is possible to identify quantities which play the equivalent role as CCP fold when performing weighted stacking for S1 and S2, based on inspection of equations (6) (offset-independent stacking) and (13) (offset dependent stacking). I illustrate the resulting "effective fold" maps for the cross-spread geometry shown in Figure 4, which is typical of OBC acquisition. Shot and receiver lines are 200 meters apart, whilst both shot and receiver spacing is 25 meters along the lines. Five orthogonal shot lines and receiver lines were used.

Figure 5 shows the conventional CCP fold map obtained from the above geometry, based upon asymptotic CCP binning, using a γ (V_P/V_S) value of 3, and binning the CCPs onto a 12.5 m x 12.5 m grid. The resulting fold is fairly uniform, not falling below 10 fold within the fully covered region. Figure 6 shows the fold maps based upon equation (6), with the fast direction parallel to the X-axis ($\phi = 0^\circ$). There are now two maps, one (a) for the "effective S1 fold", and another (b) the "effective S2

fold". Whilst the numerical values cannot be directly compared with conventional fold, due to the trigonometric factors, there is more variation spatially. The different patterns of fold variation, compared to the conventional fold map, arise due to the bin-to-bin variation in azimuth distribution and more specifically deviation from the S1 and S2 directions. Figure 7 shows the corresponding pair of S1 and S2 fold maps for $\phi = 45^o$. Note that the principal axis direction leaves an imprint on the effective fold map, indicating that it will have in influence on the acquisition footprint if uncorrected for. The S1 and S2 maps were also computed for $\phi = 90^o$. As anticipated, the results were identical to the maps for $\phi = 0^o$, but with the roles of S1 and S2 reversed, and are not shown here. Figure 8 shows the results based on the offset dependent equation (13), for an S1 azimuth $\phi = 45^o$. This should be compared with Figures 5 and 7. Again whilst direct numerical comparison is not meaningful, due to the offset factors now included, the increased variation spatially is apparent.

DISCUSSION

An important – perhaps surprising – facet of the algorithm embodied in equation (13), is that apart from the direction, ϕ, of the principal axes, *no further knowledge* of the birefringent medium is needed. We don't need to use the transmission responses or the travel delay times, anywhere, in computing the S1 and S2 stacks. Indeed it appears from equation (2) that once we have obtained the stacks U_{SS1} and U_{SS2}, we should be able to compute a transfer function to map the transmission response of one to the other. Whether this is achievable in practice remains to be demonstrated.

Whilst the above theory is based upon looking at the transmission effects on a conversion from below the birefringent layer, it can and should be extended to the analysis of reflections from within such media. This will enable the characterization of fractured media at the reservoir level, instead of simply removing overburden effects. The analysis above considers the case of a single anisotropic layer, whereas we may in practice observe changes with depth in the polarizations due for example to changes in stress regime or fracture orientation. In this case, it is probably preferable to layer strip the overburden layers, and confine the separate imaging of S1 and S2 to the reservoir. Otherwise the interpreter may be confronted with 2^N images, where N is the number of different birefringent layers!

The above derivation of S1 and S2 weighted stacking is based upon a number of assumptions that may need further examination. Firstly, the theory of S1 and S2 modes, in particular the assumption of orthogonality, is based upon near-vertical wave propagation. Likewise, as noted above, the AVO equation and the ray-parameter calculation are also near offset approximations. A challenge, therefore, is to quantify accuracy for realistic offset ranges, and if possible to extend the theory to larger offsets.

An issue which is always important to consider when performing any vector processing of X and Y component data, such as that described above, is the issue of vector fidelity. A second related issue is that of geophone orientation. Whilst these prerequisites have been assumed here, they are the goal of much ongoing work at present. A recent example of this work is Dellinger et al. (2001).

CONCLUSIONS AND FUTURE WORK

Stacking 3-D converted-wave data to obtain S1 and S2 images is more involved than for 2-D data, due to the variation in azimuth relative to the principal axes. I have developed a theoretical basis for doing so, including the effects of both azimuth and offset. There is an acquisition footprint effect that can be identified by examining the effective S1 and S2 fold maps. I have shown examples based on a cross-spread geometry.

Imaging using S1-S2 weighted stacking theory needs to be demonstrated on both model and synthetic 3-D converted-wave data. Further extensions to the theory, as mentioned above, will be pursued.

ACKNOWLEDGEMENTS

I thank sponsors of CREWES Project for their support, and WesternGeco for supporting my research at CREWES.

I thank Rob Stewart and Jim Brown for helpful discussions and for reviewing this paper.

REFERENCES

Alford, R. M., 1986, Shear data in the presence of azimuthal anisotropy: Dilley, Texas: 56th Internat.. Mtg., Soc. Expl. Geophys., Expanded Abstracts, 86, S9.6, 476-479.

Bale, R., Dumitru, G, and Probert, T., 2000, Analysis and stacking of 3-D converted-wave data in the presence of azimuthal anisotropy: 70th Annual Internat. Mtg. Soc. Expl. Geoph., Expanded Abstracts, 1189-1192.

Bale, R., Leaney, S., and Dumitru, G., 2001, Offset-to-angle transformations for PP and PS AVO analysis: 71st Annual Internat. Mtg. Soc. Expl. Geoph., Expanded Abstracts.

Dellinger, J., Clarke, R., and Gutowski, P., 2001, Horizontal vector infidelity correction by general linear transform, 71st Annual Internat. Mtg. Soc. Expl. Geoph., Expanded Abstracts, ??.

Fang, K., 1998, Pseudo-Spectral Modelling of Cracked Anisotropic Media and Rotation of Multicomponent Shear-Wave Data: M. Sc. Thesis, Univ. of Calgary.

Fang K., and Brown, R. J., 1996, A new algorithm for the rotation of horizontal components of shear-wave seismic data: CREWES Research Report, **8**, 12.1-12.14.

Gaiser, J., 2000, Advantages of 3-D P-S-wave data to unravel S-wave birefringence for fracture detection, 70th Ann. Internat. Mtg: Soc. of Expl. Geophys., 1201-1204.

Garotta, R., 1989, Detection of azimuthal anisotropy, 59th Ann. Internat. Mtg: Soc. of Expl. Geophys., 861.

Li, X.-Y., 1998, Fracture detection using P-P and P-S waves: 68th Annual Internat. Mtg. Soc. Expl. Geoph., Expanded Abstracts, 2056-2059.

Nieto, C, and Stewart, R.R., 2001, Angle of incidence estimation for converted-wave AVO analysis: CREWES Research Report, **13**.

Probert, T. and Wells, S., 2000, The Gryphon 4C survey - processing and results: 62nd Mtg. Eur. Assn. Geosci. Eng., Session: L0006.

Stewart, R.R., Zhang Q., and Guthoff, F., 1995, Relationships among elastic-wave values (R^{PP}, R^{PS} , R^{SS},V_P, V_S, ρ, σ, κ): CREWES Research Report, **7**, 12.1-12.5.

Tessmer, G. and Behle, A., 1988, Common reflection point data-stacking technique for converted waves: Geophysical Prospecting, **36**, 671-688.

Thomsen, L., 1988, Reflection seismology over azimuthally anisotropic media: Geophysics, **53**, 304-313.

Thomsen, L., 1999, Converted-wave reflection seismology over inhomogeneous, anisotropic media: Geophysics, **64**, 678-690.

Walden, A. T., 1991, Making AVO sections more robust: Geophys. Prosp., **39**, 915-942.

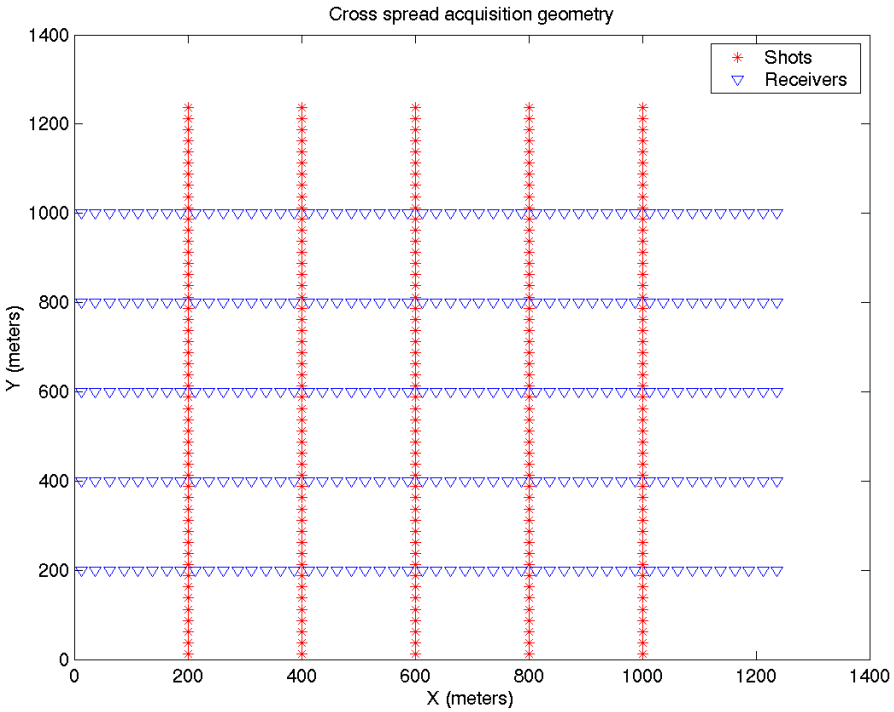

FIG. 4. Cross-spread acquisition geometry for fold study. Shot and receiver spacing is 25m.

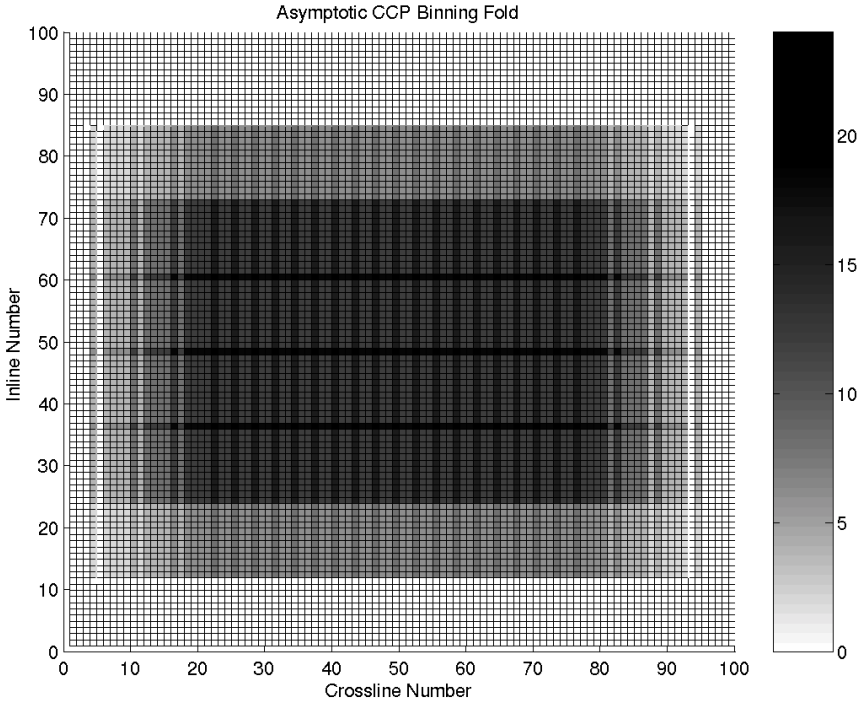

FIG. 5. Fold map for 12.5 x 12.5 meter binning, based on asymptotic binning with γ=3.

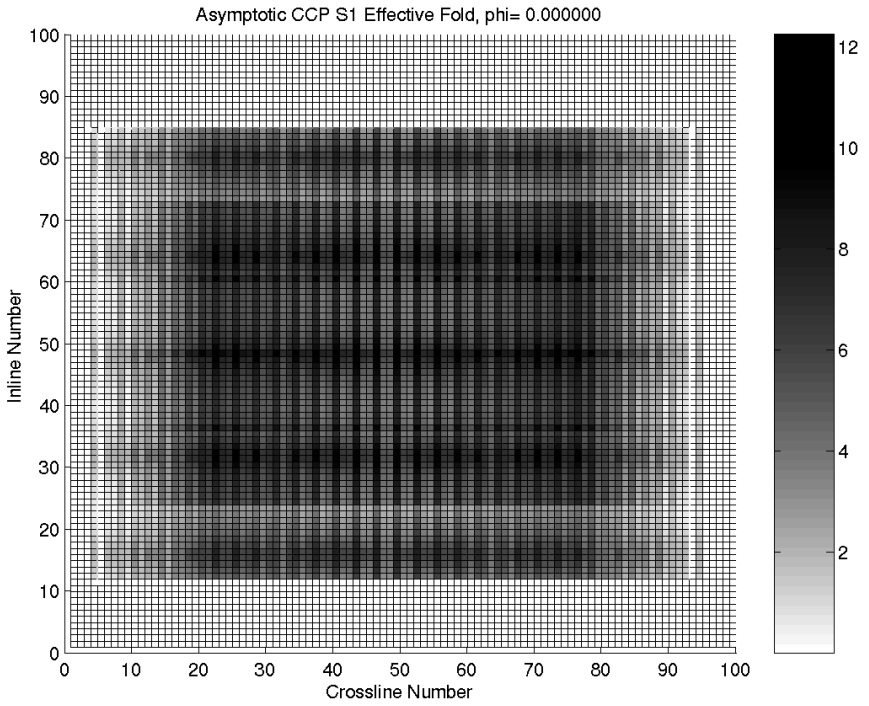

FIG. 6(a). Effective S1 fold computed from $\sum_{i=1}^{N} \cos^2(\theta_i - \phi)$, with $\phi = 0°$.

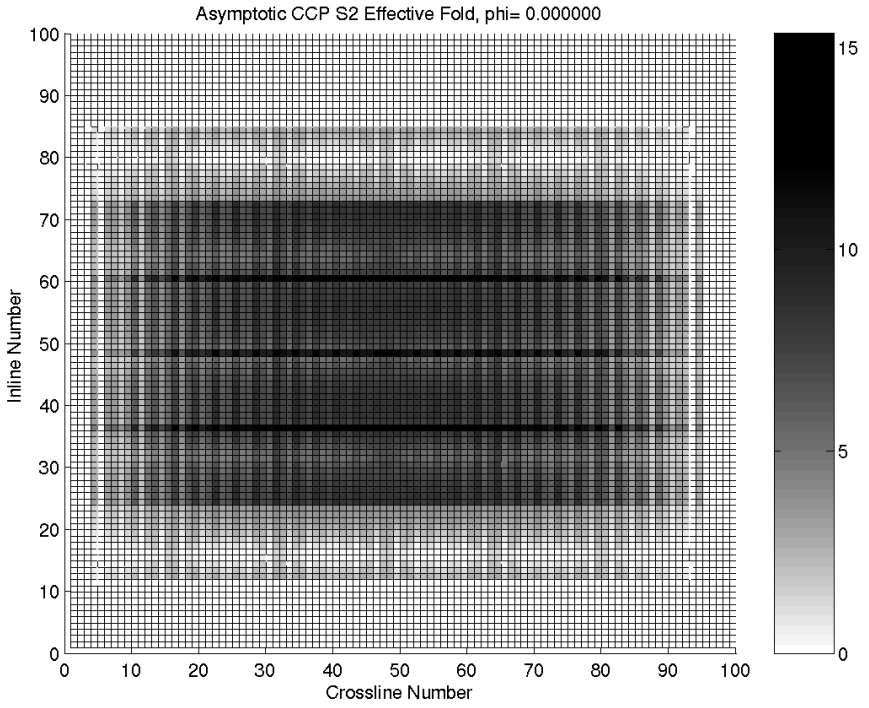

FIG. 6(b). Effective S2 fold computed from $\sum_{i=1}^{N} \sin^2(\theta_i - \phi)$, with $\phi = 0°$.

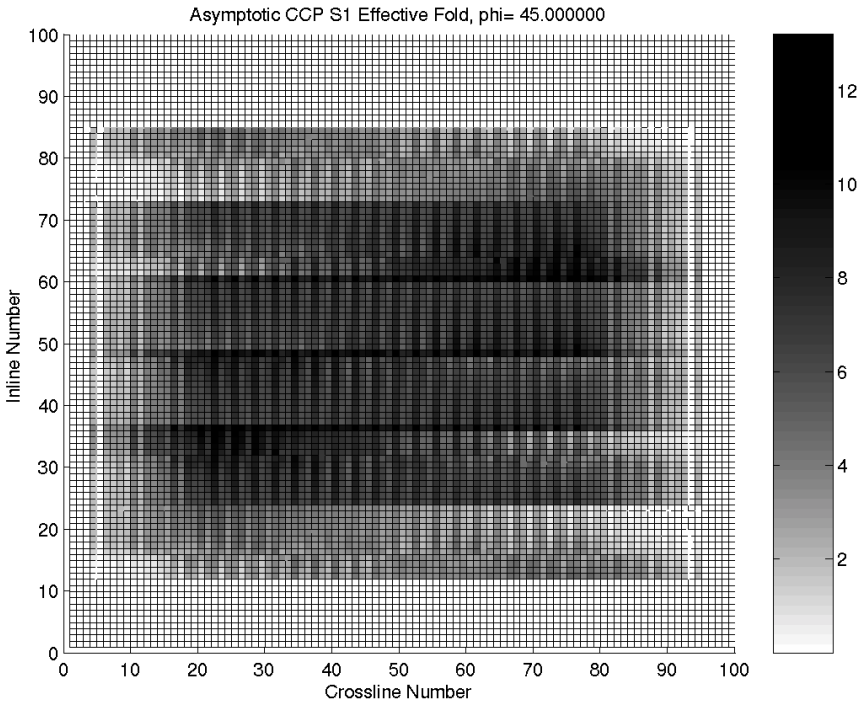

FIG. 7(a). Effective S1 fold computed from $\sum_{i=1}^{N} \cos^2(\theta_i - \phi)$, with ϕ = 45°.

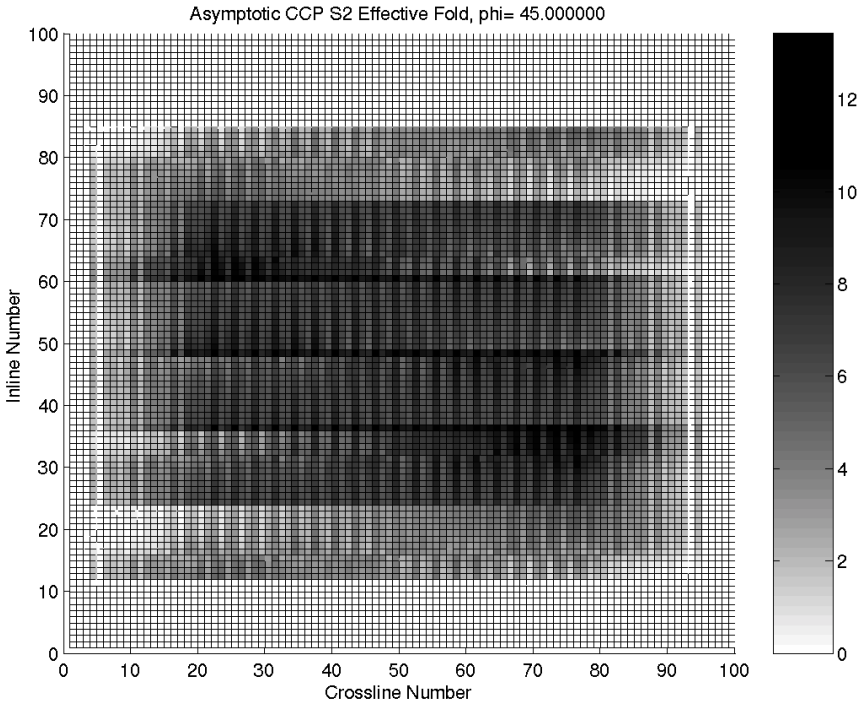

FIG. 7(b). Effective S2 fold computed from $\sum_{i=1}^{N} \sin^2(\theta_i - \phi)$, with ϕ = 45°.

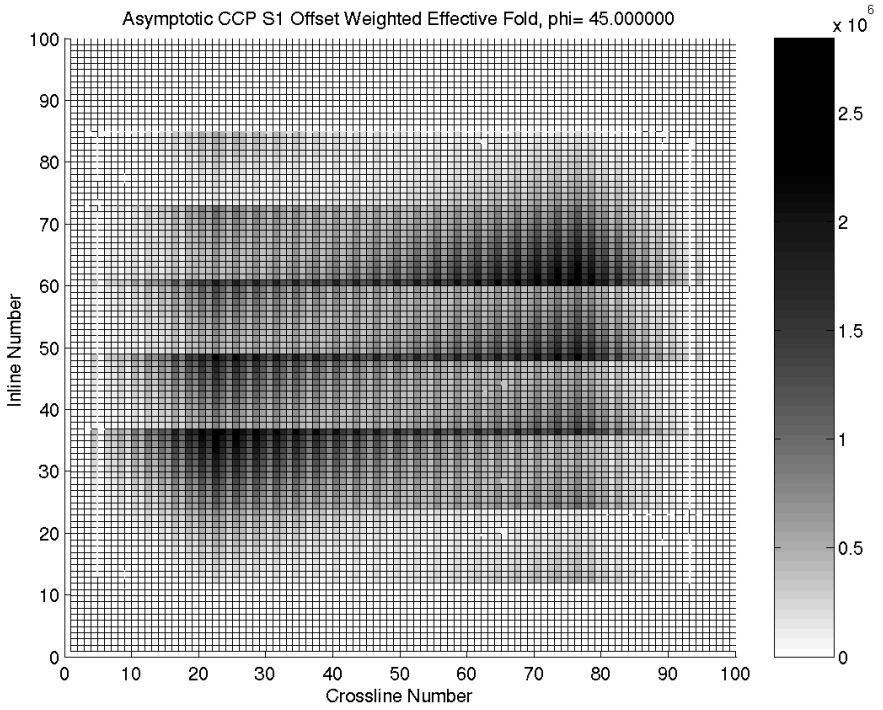

FIG. 8(a). Effective S1 fold computed from $\sum_{i=1}^{N}\left(\frac{r_i}{t}\right)^2 \cos^2(\theta_i - \phi)$, with ϕ = 45°.

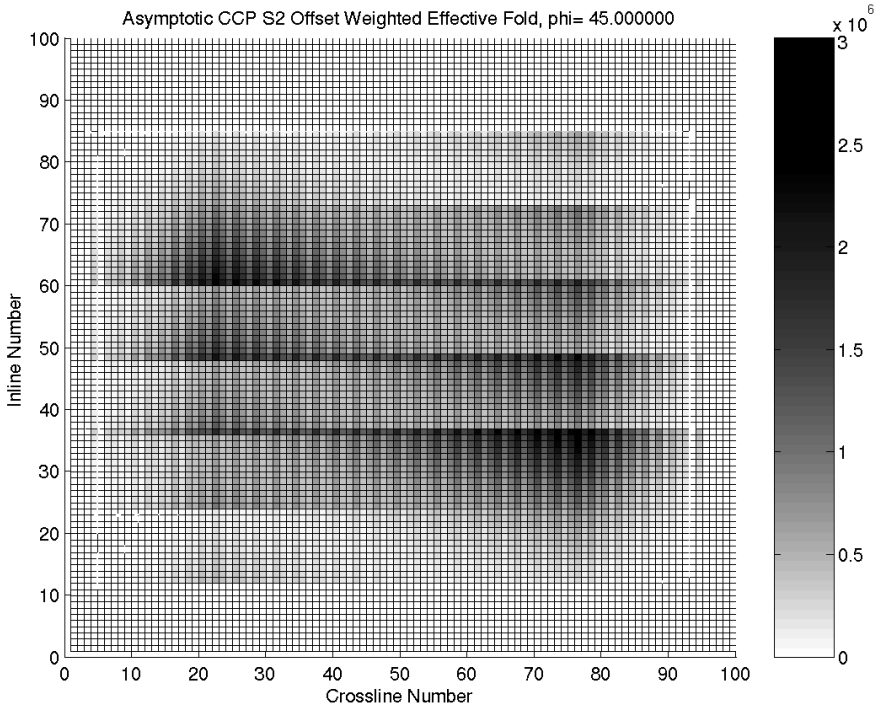

FIG. 8(b). Effective S2 fold computed from $\sum_{i=1}^{N}\left(\frac{r_i}{t}\right)^2 \sin^2(\theta_i - \phi)$, with ϕ = 45°.